ELSEVIER

Contents lists available at ScienceDirect

## Microchemical Journal

journal homepage: www.elsevier.com/locate/microc



# Enhanced dual fluorescence quenching of red and blue emission carbon dots by copper dimethyldithiocarbamate for selective ratiometric detection of ziram in foodstuff and water samples

Khalid Alhazzani <sup>a</sup>, Ahmed Z. Alanazi <sup>a</sup>, Aya M. Mostafa <sup>b,c</sup>, James Barker <sup>b</sup>, Hossieny Ibrahim <sup>d,e</sup>, Mohamed M. El-Wekil <sup>c</sup>, Al-Montaser Bellah H. Ali <sup>c,\*</sup>

- <sup>a</sup> Department of Pharmacology and Toxicology, College of Pharmacy, King Saud University, Riyadh, Saudi Arabia
- <sup>b</sup> School of Life Sciences, Pharmacy, and Chemistry, Kingston University, Kingston-upon-Thames, London KT1 2EE, UK
- <sup>c</sup> Department of Pharmaceutical Analytical Chemistry, Faculty of Pharmacy, Assiut University, Assiut, Egypt
- <sup>d</sup> Department of Chemistry, Faculty of Science, Assiut University, Assiut 71516, Egypt
- e School of Biotechnology, Badr University in Assiut, Assiut 2014101, Egypt

#### ARTICLE INFO

Keywords: Ziram Carbon dots, Quenching Copper dimethyldithiocarbamate Copper ions

#### ABSTRACT

The monitoring of ziram levels is of vital importance due to its widespread application in agriculture and the possible risks it poses to human health and the ecosystem. This work proposes an innovative approach for the highly sensitive and selective sensing of ziram, a widely used dithiocarbamate fungicide, through the formation of copper dimethyldithiocarbamate Cu)DDC)2 assisted dual quenching of red and blue emission carbon dots (R/ NCDs and B/NSCDs). When ziram is added to a system containing copper-bound B/NSCDs and R/NCDs, the displacement of ziram zinc ions by copper ions leads to the formation of a yellow-colored Cu)DDC)2 complex. This complex induces significant quenching of the fluorescence emissions from both types of carbon dots, consequently enhancing the sensitivity of the detection method. Comprehensive characterization of the R/NCDs and B/NSCDs was conducted using various spectroscopic and morphological techniques to elucidate their structural and optical properties. The quenching mechanism was confirmed through different spectroscopic techniques, including fluorescence lifetime measurements, UV-vis spectroscopy, and Stern-Volmer analysis. The proposed method demonstrated high sensitivity across a wide concentration ranging from 20 to 1000 ng mL<sup>-1</sup> making it suitable for trace-level detection of ziram. Moreover, the method exhibited excellent selectivity and recovery when applied to real samples, such as apples, grains, and water matrices. The combination of high sensitivity, selectivity, and applicability to diverse sample matrices makes this carbon dot-based dual quenching method a promising approach for fast and accurate detection of ziram in various environmental and agricultural applications.

#### 1. Introduction

Ziram, also known as zinc dimethyldithiocarbamate, is an organosulfur compound widely used as a fungicide [1]. Ziram is widely employed as a broad-spectrum fungicide in agricultural applications to manage fungal diseases in a diverse range of crops, vegetables, and ornamental plants [2]. It is particularly effective against a wide range of fungal pathogens, including downy mildews, rusts, and blights. Additionally, ziram is used as an accelerator in rubber industry, where it facilitates the vulcanization process and improves the physical properties of rubber products [3]. Despite its extensive use, residues of ziram and its degradation byproducts have the potential to present risks to both human well-being and ecological balance [4]. Ziram has been categorized as a probable carcinogenic substance for humans by the United States Environmental Protection Agency (EPA), and it has been linked to several detrimental health impacts, such as impairments in developmental processes, neurotoxic effects, and disruptions in reproductive functions [5,6]. Exposure to ziram can occur through occupational settings, dietary sources, or environmental contamination [7]. Ziram has been detected in soil, water bodies (surface water, groundwater, and sediments), air, and even in food products treated with ziram [8]. One notable property of ziram is its ability to complex with metal

E-mail address: Almontaser\_bellah@aun.edu.eg (A.-M. Bellah H. Ali).

<sup>\*</sup> Corresponding author.

ions, particularly those of a soft nature, such as copper, lead, and mercury [9]. This complexation can occur through the interaction of the dithiocarbamate moieties in ziram with the metal ions, forming stable metal-dithiocarbamate complexes [10,11]. The detection of ziram residues holds significant importance for safeguarding societal health.

Previous analytical techniques employed for ziram detection, such as gas chromatography (GC) [12], UV-Vis spectrophotometric analysis [13], and FT-IR spectroscopic analysis [14], primarily depend on the application of large-scale and intricate analytical instrumentation. While these methods offer high sensitivity for ziram detection, they often involve complex analytical procedures. Typically, these methods require an initial acid hydrolysis step to convert ziram into carbon disulfide (CS2), followed by instrument-based detection. A different method encompasses extracting, concentrating, and then detecting compounds through liquid chromatography [15]. Although this method can directly detect ziram, it often needs derivatization due to the compound's instability [16]. Other techniques, such as flame atomic absorption analysis [17], voltammetry [18], and inductively coupled plasma-mass spectroscopy [19], can also be employed for ziram sensing. But, these methods are susceptible to interference from substances containing zinc, as they primarily rely on indirectly analyzing the zinc content present in ziram.

Photochemical techniques have demonstrated successful implementation in the analysis of residual traces of organophosphorus and carbamate-based pesticides, utilizing different enzymes as the basis for detection [20]. However, the potent indiscriminate chelating characteristics of ziram pose significant challenges for the application of optical enzyme-based chemosensors in its detection. To address this limitation, researchers have investigated alternative photometric method utilizing gold nanoparticles for the analysis of pesticide residues [21]. While these approaches have garnered significant attention, the extent of gold nanoparticle aggregation, which induces alterations in the optical characteristics, may cause inaccuracies in the detection of ziram concentrations. Copper nanoparticles have also been investigated as fluorometric probes for the sensing of pesticide residues [22]. Nevertheless, the practical applicability of these nanoparticles is severely limited due to their inherent instability. Given the limitations of existing photochemical methods and the need for accurate and reliable ziram detection, there is a pressing demand for the development of new fluorometric probes that exhibit high selectivity and sensitivity [23-25].

Despite the advancements in analytical techniques for ziram detection, there remains a need for a simple, cost-effective, and highly selective method that can address the limitations of existing approaches. The proposed method in this work addresses these challenges by employing a novel dual quenching strategy involving red and blue emission carbon dots, which exhibits high sensitivity and selectivity for ziram detection without the need for complex instrumentation or sample pretreatment, making it a promising alternative to conventional techniques.

Carbon dots (CDs) are a class of fluorescent, quasi-spherical nanoparticles typically ranging from 2 to 10 nm in size, consisting of a carbon-based core and surface functional groups [26,27]. They offer excellent optical properties, including tunable fluorescence emission, high photostability, and broad excitation spectra, making them appealing for numerous applications such as bioimaging and biosensing, [28–32]. CDs exhibit low toxicity, good biocompatibility, and excellent water solubility, suitable for biological and environmental applications [33]. CDs serve as fluorescent probes for detecting biomolecules [33], pesticides [34,35], fungicides [36], herbicides [37,38], and ions. CDs can be prepared through top-down methods involving the breakdown of larger carbon-based materials or bottom-up methods synthesizing them from small molecular precursors through pyrolysis, hydrothermal treatment, or microwave-assisted synthesis, with the choice of synthesis method and precursor materials significantly influencing their properties and performance [39,40].

The novelty of this work lies in the innovative strategy of leveraging

the dual fluorescence quenching response of nitrogen-doped red emissive carbon dots (R/NCDs) and blue emissive nitrogen and sulfur-doped carbon dots@copper (B/NSCDs@Cu) for the highly sensitive and selective ratiometric sensing of ziram. This approach is based on the unique optical characteristics of carbon dots and their ability to undergo efficient quenching by the copper dimethyldithiocarbamate (CuDDC)2 complex formed upon the displacement of zinc ions from ziram. The proposed method utilizes a ratiometric strategy based on measuring the difference between the quenched signals from R/NCDs and B/ NSCDs@Cu, then dividing it against the corresponding difference in the blank readings. The implementation of a dual quenching response is pivotal in enabling this ratiometric approach. By monitoring the quenching of two distinct carbon dot emissions, the method can account for potential variations in individual signal intensities caused by factors such as instrument fluctuations or sample matrix effects. The ratiometric signal, derived from the normalized difference between the quenched emissions, becomes less susceptible to these external influences, thereby enhancing the quantitative accuracy and reproducibility of the detection method. Moreover, the dual quenching response provides an additional layer of selectivity, as the quenching patterns observed for R/NCDs and B/NSCDs@Cu can be tailored to the specific analyte of interest, minimizing potential interferences from other species. This selectivity, combined with the robustness of the ratiometric approach, contributes to the overall reliability and practical applicability of the proposed approach in environmental and agriculture applications. Although most traditional ratiometric probes rely on one invariant fluorophore and another with a changing response or two fluorophores with opposite changes, the term "ratiometric" has been used in several previous studies for dual quenching systems similar to our approach. In these systems, the ratio of the quenched fluorescence intensities from two different fluorophores is utilized for sensing [41-43].

# 2. Experimental

### 2.1. Materials and reagents

Semicarbazide, sulfosalicylic acid, O-phenylenediamine (OPD), ethylenediamine, and copper sulphate were obtained from El-Nasr Pharmaceutical Chemicals Co., Cairo, Egypt. Hydrochloric acid (HCl), boric acid (H $_3$ BO $_3$ ), acetic acid (CH $_3$ COOH), phosphoric acid (H $_3$ PO $_4$ ), and sodium hydroxide (NaOH) were procured from alpha chemika Co., India. Insecticides and fungicides standards, including ziram (>99.0 %), chlorothalonil (98 %), fipronil ( $\geq$ 98 %), captan (98 %), chlorpyrifos (99 %), myclobutanil (98 %), molosultap (98 %), azoxystrobin (97 %), folpet (>98.0 %), parathion (>98.0 %), metalaxyl (99 %), and imidacloprid (98.5 %) were procured from Sigma Aldrich (Steinheim, Germany). We used the chemicals as they came, without further purification. For all experiments, Milli-Q double-distilled water (DDW) with a resistivity of 18.2 M $\Omega$ .cm was used.

## 2.2. Instrumentation

Instrumentation can be found in the Supplementary Data file.

## 2.3. Synthesis of R/NCDs and B/NSCDs

The preparation of R/NCDs and B/NSCDs followed previously reported procedures with some modifications [44]. The preparation of the R/NCDs fluorescent nanoparticles was conducted through a hydrothermal approach, utilizing semicarbazide and o-phenylenediamine (OPD) as precursor materials. In the initial step, a specific quantity of semicarbazide (0.5 g) and OPD (1.0 g) were suspended in 50 mL of DDW to form a homogeneous mixture. The resulting mixture was subsequently moved to a hydrothermal autoclave with a Teflon lining, where the heating of the samples was maintained at 180 °C for an extended time frame of 6 h. Once the heating was finished, the autoclave was left

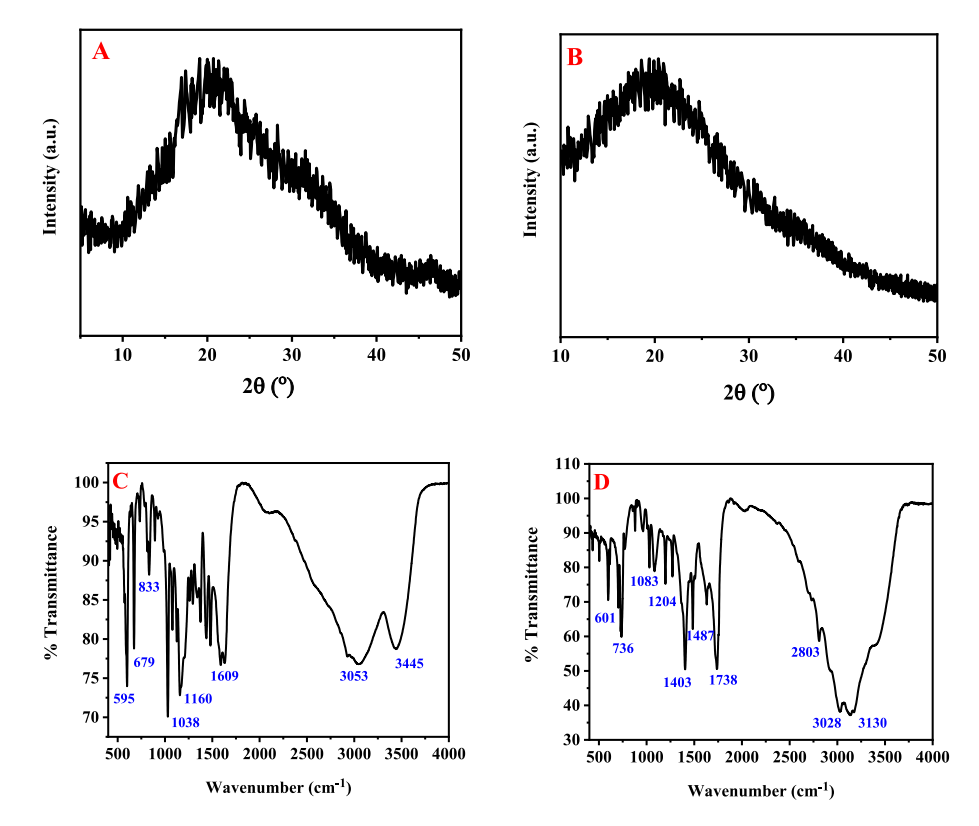


Fig. 1. XRD pattern of (A) B/NSCDs and (B) R/NCDs and FT-IR spectra of R/NCDs (C) and (D) B/NSCDs.

to cool until it reached room temperature. The resulting solution underwent centrifugation at a rotational speed of 8000 rpm for 20 min to separate the solid and liquid phases. Following this, the supernatant underwent careful filtration utilizing a 0.22  $\mu m$  syringe filter. The filtered solution then underwent a dialysis process, where it was enclosed in a 1000 Da dialysis bag and dialyzed against water for 24 h. Finally, the dialyzed solution was subjected to a freeze-drying process. This powdered material was then kept at a temperature of 4  $^{\circ} C$ .

The synthesis of B/NSCDs was accomplished via a hydrothermal strategy, employing sulfosalicylic acid and ethylenediamine as the precursor materials. In the initial step, specific quantities of sulfosalicylic acid (0.2 g) and ethylenediamine (0.2 mL) were suspended in 50 mL of DDW to form a homogeneous solution. This suspension was then placed in a Teflon-lined hydrothermal autoclave and exposed to an elevated temperature of 180  $^{\circ}\text{C}$  for six hours. Following the completion of the heating, the autoclave was allowed to cool down naturally until it reached room temperature. The resulting dispersion was subjected to centrifugation at a rotational speed of 8000 rpm for 10 min. The supernatant obtained after centrifugation was carefully filtered through a 0.22 µm syringe filter. The filtered solution underwent a dialysis process, wherein it was moved to a 1000 Da dialysis bag and dialyzed against water for a period of 24 h. Lastly, the dialyzed solution was subjected to a lyophilization (freeze-drying) process. This powdered product was then kept at a temperature of 4 °C.

Briefly, for both R/NCDs and B/NSCDs, the synthesis involved mixing precursors in DDW, autoclaving at 180  $^{\circ}$ C, followed by cooling, centrifugation, filtration, dialysis, and freeze-drying. The R/NCDs used semicarbazide and OPD as precursors, while B/NSCDs were synthesized from sulfosalicylic acid and ethylenediamine. Final products were subsequently stored at 4  $^{\circ}$ C.

# 2.4. Quantum yield of the prepared CDs

For quantum yield calculations, refer to the Supplementary Data file.

#### 2.5. Determination of ziram

To determine ziram concentration utilizing the developed method, 1.0~mL of B/NSCDs stock solution (0.05 mg mL $^{-1}$ ), 1.0~mL of Cu $^{2+}$  stock solution (100.0 µg mL $^{-1}$ ), and 1.0 mL of R/NCDs stock solution (0.1 mg mL $^{-1}$ ) were added to a 10.0 mL volumetric flask. Following that, 1.0 mL of different concentrations of ziram were transferred and left to stand for 1.0 min. A blank solution was prepared by adding 1.0 mL of DDW instead of ziram. For each flask, the desired volume was achieved by topping up with a buffer solution (B.R.) maintained at a pH of 7.0. The photoluminescence spectra were obtained by exciting the samples at a wavelength of 280 nm, and the photoluminescence intensities were measured at 400 nm and 610 nm, which correspond to the respective emission peaks of B/NSCDs and R/NCDs.

### 2.6. Determination of ziram in water samples, apple and wheat grains

Water samples from various sources, including tap water and river water, were gathered from the city of Assiut, Egypt. Water samples first underwent a two-step pretreatment process. Initially, filtration was carried out utilizing a cellulose membrane filter, with a pore size of 0.45  $\mu m$ . This was followed by an ion exchange treatment to remove potential interfering metal ions, particularly copper, which may affect the accuracy of the determination procedures.

The determination of ziram in apple fruits entailed an extraction procedure following the procedures suggested by Luo et al [45]. The apple fruits underwent peeling, cutting into smaller pieces, and homogenization at a speed of 12,000 rpm. Subsequently, varying concentrations of ziram were deliberately introduced into the homogenized fruit samples. To extract ziram, A quantity of 5.0 g of the sample, spiked with ziram, was combined with 5.0 ml of a solution comprising 50 % acetonitrile and 50 % water, along with 2.0 g of sodium acetate trihydrate. This mixture was vigorously shaken for 1.5 min to facilitate extraction. After shaking, the mixtures underwent centrifugation at 12,000 rpm for a duration of 4 min, after which the supernatant fraction

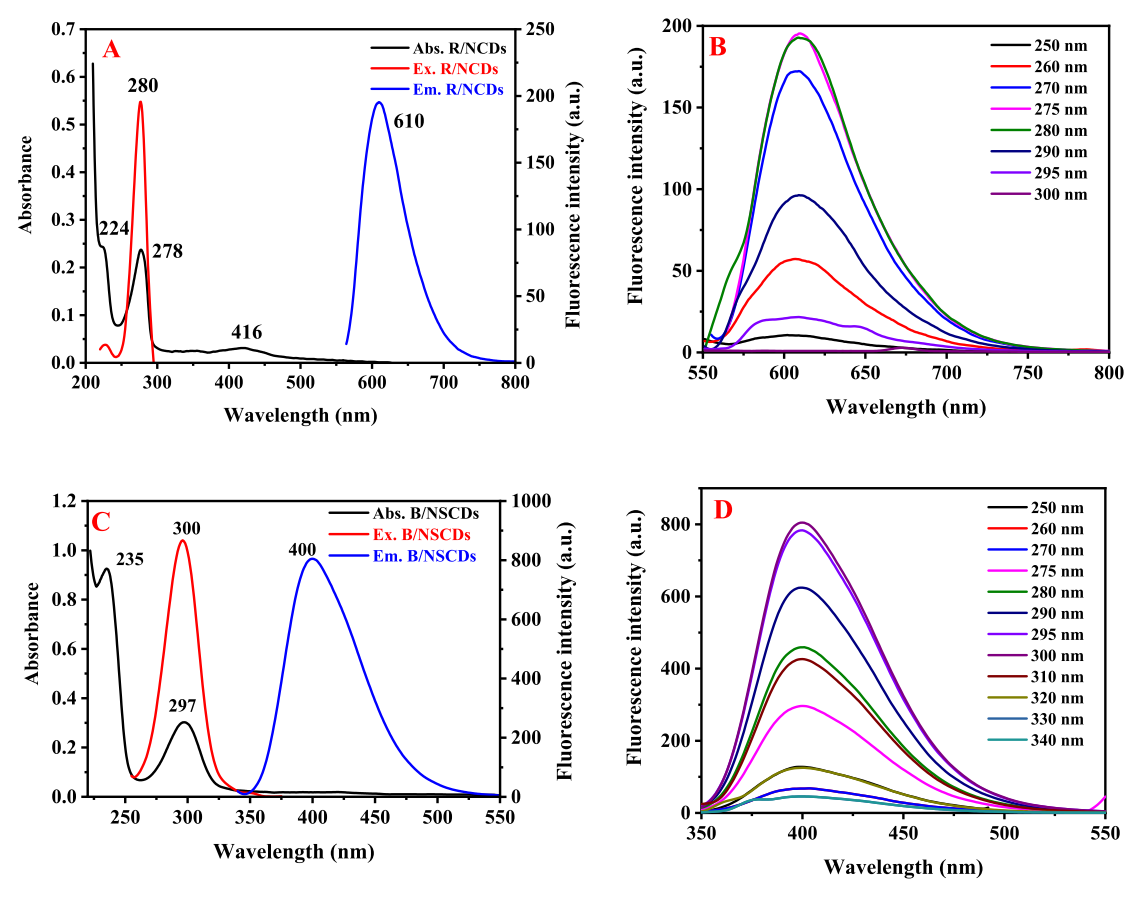


Fig. 2. (A) UV-visible absorption, excitation, and emission spectra of R/NCDs, (B) Emission spectrum of R/NCDs under excitation from 250 to 300 nm, (C) UV-visible absorption, excitation, and fluorescence spectra of B/NSCDs, (D) Emission spectrum of B/NSCDs under excitation from 250 to 340 nm.

was collected. To mitigate potential interferences from food components such as organic acids, sugar, and pectin, a transfer of 3 mL of the collected supernatant was conducted into a separate test tube with a capacity of 10 mL. Subsequently, 0.45 g of adsorbents (specifically, octadecylsilane silica/primary-secondary amine adsorbent or PSA/C18) was added to the test tube and mixed thoroughly. This mixture underwent centrifugation again at 12,000 rpm, and the final supernatant was collected in a separate test tube. The resulting supernatant was subjected to filtration using 0.20  $\mu m$  nylon filters, and the filtered solution was then analyzed using the designed method for ziram detection.

Wheat grain samples were prepared by accurately weighing approximately 10.0 g of finely ground wheat grains. Subsequently, the grains were subjected to spraying with aqueous suspensions containing different amounts of ziram. After spraying, the treated samples were left to dry under direct sunlight for one hour, followed by additional drying in the shade for 24 h to evaporate any excess moisture. The dried wheat samples were soaked in 50.0 mL of a 0.1 M NaOH solution and were left standing for a duration of 10 min. The mixture was then spun in a centrifuge at 2000 rpm for five minutes. After filtering aliquots of the solutions, their pH was brought to neutral by the addition of 0.1 M HCl [46]. Finally, the neutralized aliquots were analyzed following the general procedure outlined for the analytical method.

## 3. Results and discussion

### 3.1. Characterization of CDs

TEM imaging was used to investigate the morphology and particle size of B/NSCDs and R/NCDs (Fig. S1A and B). The TEM images revealed that both types of carbon dots exhibited a spherical shape and relatively uniform size distribution. The insets of the respective TEM

images indicated that the average diameters were approximately 3.5 nm for B/NSCDs and 3.0 nm for R/NCDs. Further characterization was performed using XRD analysis. The XRD patterns displayed distinct broad peaks for both B/NSCDs and R/NCDs, indicating that these carbon dots primarily consist of an amorphous core structure. XRD patterns exhibited peaks associated with the (002) plane of the graphitic structure, which were centered at approximately 20.7° for B/NSCDs and 20.2° for R/NCDs (Fig. 1A and B) [28].

FT-IR spectra revealed important details regarding the functional groups found on the surfaces of R/NCDs and B/NSCDs. For R/NCDs (Fig. 1C), the split broad peak at 3445 cm<sup>-1</sup> and 3053 cm<sup>-1</sup> was attributed to the vibrational stretching of O-H and N-H bonds, respectively [29]. The peaks at 1609 cm<sup>-1</sup> and 1160 cm<sup>-1</sup> were attributed to the stretching oscillations of C = N and C-N bonds, respectively, while the band at 1038 cm<sup>-1</sup> corresponded to the stretching modes of C-O bonds [27]. Additionally, the signal at 833 cm<sup>-1</sup> was associated with the bending oscillation of N-H group, and the peaks at 679 cm<sup>-1</sup> and 595 cm<sup>-1</sup> were ascribed to the bending oscillations of C-H bonds. On the other hand, the FT-IR spectrum of B/NSCDs (Fig. 1D) revealed different functionalities on its surface. The forked broad peaks at 3130 cm<sup>-1</sup> and 3028 cm<sup>-1</sup> were linked to the oscillational stretching of OH and NH groups, respectively, while the small signal at 2803 cm<sup>-1</sup> reflected the stretching oscillations of C-H groups. The sharp band at 1738 cm<sup>-1</sup> was corresponding to the vibrational stretching of carbonyl groups, and the peaks at 1487 and 1403 cm<sup>-1</sup> were assigned to the stretching modes of C = N and C-N groups, respectively [32,47]. Additionally, the small peak at 1204 cm<sup>-1</sup> was related to the vibrational stretching of C-O bonds, and the signal at  $1083 \text{ cm}^{-1}$  was related to the stretching oscillations of S = O bonds [28]. The sharp band at 736 cm<sup>-1</sup> was associated with the vibrational bending of N-H bond, while the signal at 601 cm<sup>-1</sup> was ascribed to the bending oscillations of C-H bond. XPS was utilized to investigate the elemental composition of both B-NS@CDs and R-N@CDs. XPS spectroscopic examination showed that R-N@CDs were composed of C, N, and O atoms (Fig. S1C), while B-NS@CDs contained C, N, O, and S atoms (Fig. S1D) [32].

#### 3.2. Spectroscopic properties of CDs

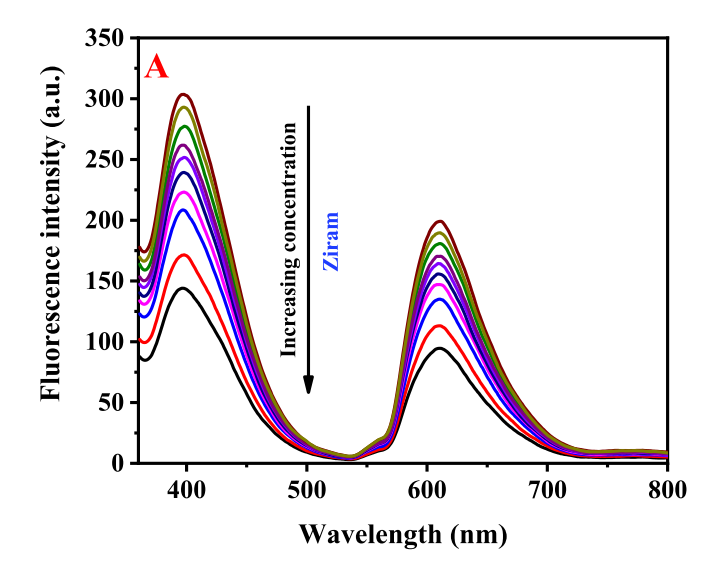
The spectroscopic properties of R/NCDs and B/NSCDs were investigated using ultraviolet-visible spectroscopy and fluorescence spectroscopic measurement. For R/NCDs, the UV-Vis absorption spectrum (Fig. 2A) displayed a shoulder peak at 224 nm, related to  $\pi$  to  $\pi^*$  transition, and an intense peak at 278 nm, indicating n to  $\pi^*$  transition [32]. Moreover, a wide absorption peak centered at 416 nm suggests that there are prolonged conjugated frameworks or the development of more extensive aromatic regions within the carbon nanodots. The fluorescence emission spectrum of R/NCDs displayed a maximum emission band at 610 nm after excitation at 280 nm (Fig. 2A). It's worth noting that the emission at 610 nm remained consistent, regardless of the excitation wavelengths used within the range of 250 to 300 nm. This observation suggests the existence of a single emissive state or a narrow distribution of emissive sites within the carbon dots [48]. Regarding B/ NSCDs, the UV-visible absorption spectrum (Fig. 2C) has a small peak at 235 nm, related to  $\pi$ - $\pi$ \* transition, and an intense absorption band at 297 nm, reflective of  $n-\pi^*$  transition of carbonyl group, imine group, or the exitance of heteroatom-containing aromatic moieties [31]. The fluorescence emission spectrum of B/NSCDs displayed a maximum fluorescence peak at 400 nm after excitation at 300 nm, confirming successful energy transfer and radiative recombination process within the carbon dots [31]. As with the R/NCDs, the B/NSCDs showed an emission at 400 nm that was unaffected by changes in excitation wavelengths from 250 to 340 nm (Fig. 2D). The quantum yield of R/ NCDs is 12 %, while the quantum yield of B/NSCDs is 16 %.

#### 3.3. Fluorescence stability of CDs

The fluorescence durability of both B/NSCDs and R/NCDs was examined across various pH levels, ionic strengths, and durations of UV light exposure. The effect of pH on the fluorescence intensity was examined within the interval from 2.0 to 10.0 (Fig. S2A and B). The maximum fluorescence intensity for both types of carbon dots was observed around pH 7.0. However, a decline in photoluminescence intensity was identified in highly acidic environments. This change in fluorescence with pH can be linked to either the protonation or deprotonation of functional groups on the carbon dots' surfaces [49], which can influence their electronic structure and fluorescence capabilities. The impact of ionic strength on the stability of fluorescence was assessed by varying NaCl concentrations from 0.01 to 3.0 M (Fig. S2C and D). Notably, even with increased ionic strength, the photoluminescence intensity for both B/NSCDs and R/NCDs was stable, indicating their resilience in solutions of differing ionic strengths. Furthermore, the study evaluated the photostability of the carbon dots by subjecting them to prolonged UV irradiation for a duration of up to 5.0 h (Fig. S2E and F). Despite prolonged exposure to UV irradiation, both B/NSCDs and R/ NCDs showed no significant decrease in fluorescence intensity, demonstrating their remarkable photostability. These results suggest that the synthesized B/NSCDs and R/NCDs possess remarkable fluorescence stability under varying conditions, making them promising for potential use in various fields.

#### 3.4. Optimization of reaction conditions

The optimization of experimental parameters for the fluorescence-based detection of ziram was conducted by employing a ratiometric approach. This approach involved measuring the ratio between the difference in the quenched fluorescence intensities of both R/NCDs and B/NSCDs upon exposure to ziram, divided by the corresponding



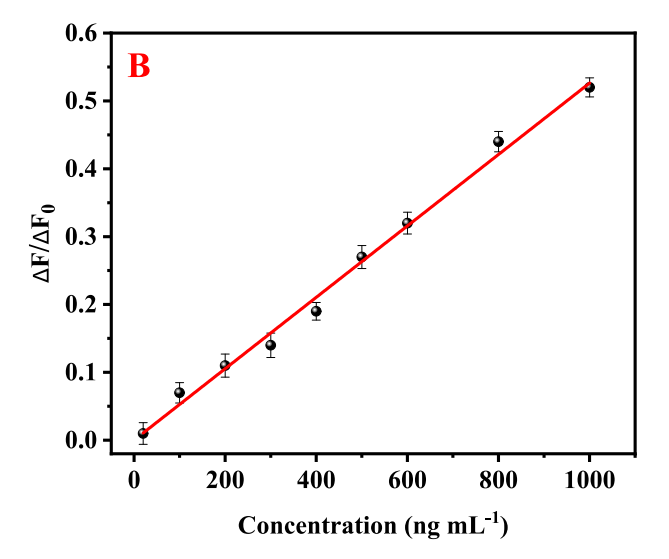


Fig. 3. (A) Fluorescence emission spectra of R/NCDs and B/NSCDs@Cu with different amounts of ziram. (B) Linear relationship of  $\Delta F/\Delta F_0$  versus ziram amounts ranged from 20.0 to 1000.0 ng mL<sup>-1</sup>. All tests were carried out in triplicate, and the error bars show the standard deviation of these triple measurements.

difference in their blank readings. Different reaction times were evaluated, ranging from 0.5 to 10.0 min. It became clear that a reaction time of 1.0 min was sufficient to achieve the highest response (Fig. S3A). The influence of pH was examined across a range of pH values from 2.0 to 8.0 (Fig. S3B). The optimum response was observed at pH 7.0. The choice of pH 7.0 as the optimum pH was related to the solubility and complexation behavior of the metal ions involved. At pH values higher than 8, Cu<sup>2+</sup> tend to precipitate as insoluble copper hydroxide species. Therefore, the investigation of pH was limited to a maximum value of pH 8 to avoid precipitation of Cu<sup>2+</sup>. Therefore, highly alkaline conditions may hinder the formation of soluble copper complexes with ziram. Conversely, highly acidic media may weaken the complexation of Cu<sup>2+</sup> with ziram. Therefore, to maintain the solubility and favorable complexation of Cu<sup>2+</sup> with ziram while minimizing the risk of precipitation, an optimal pH value around pH 7.0 is typically chosen. The amount of Cu<sup>2+</sup> was optimized within a concentration range of 1.0 to 100.0 µg mL<sup>-1</sup> (Fig. S3C), considering two factors: achieving slight fluorescence quenching for B/NSCDs and the formation of a yellow color complex that leads to significant quenching for both B/NSCDs and R/

**Table 1**Comparison of the proposed fluorescent system with other reported methods for the quantitation of ziram.

Method	Linear range ( $\mu g \ mL^{-1}$ )	LOD (µg mL <sup>-1</sup> )	Matrix	Ref.
(Fluorometric) CdSe/ZnS QDs	$1.53 \times 10^{-5}$ – $1.22 \times 10^{-2}$	$6.12 \times 10^{-6}$	Tomato and rice	[50]
(Fluorometric) Red CDs	0.0-5.0	0.55	Tap and lake water	[25]
(Fluorometric) CsPbBr <sub>3</sub> QDs	0.1–50	0.086	Apple and cherry tomato	[51]
SERS	0.01-100.0	0.01	Apple juice	[52]
SERS	0.1–10.0	0.015	Apple and pear fruits	[53]
Flame-AAS	0.08–1.6	0.145	Fog-water samples	[8]
Spectrophotometric (SCN <sup>-</sup> -rhodamine 6G)	0.05–1.0		Water, potato, cabbage and wheat grains	[54]
B/NSCDs@Cu and R/ NCDs	0.02–1.0	0.006	Apple, grains, and water	This work

NCDs. Among the tested concentrations, it was found that  $10.0~\mu g~mL^{-1}$  resulted in significant fluorescence quenching for both peaks upon addition of ziram while causing slight quenching before the addition of ziram. Although a lower response was noticed for B/NSCDs at an excitation wavelength of 280 nm, this wavelength was still chosen for both R/NCDs and B/NSCDs. The decision was based on the fact that it was the only suitable wavelength that resulted in sufficient emission for both

types of CDs.

#### 3.5. Ratiometric detection of ziram

The performance of the B/NSCDs@Cu (400 nm) and R/NCDs (610 nm) ratiometric fluorescence system for the detection of ziram was evaluated by measuring the ratio between the difference ( $\Delta F$ ) in the quenched fluorescence intensities of R/NCDs and B/NSCDs@Cu upon exposure to ziram, divided by the corresponding difference in their blank readings ( $\Delta F_0$ ), at different concentrations of ziram under optimal conditions. The fluorescence intensity ratio  $\frac{\Delta F}{\Delta F_0}$  is calculated using the formula  $\Delta F = F_{610} - F_{400}$  where  $F_{610}$  is the fluorescence intensity of R/ NCDs after exposure to ziram, and  $F_{400}$  is the fluorescence intensity B/ NSCDs@Cu after exposure to ziram. Similarly,  $\Delta F_0$  is defined as  $F_0$  $_{(610)}$ – $F_{0(400)}$ , where  $F_{0(610)}$  and  $F_{0(400)}$  are the fluorescence intensities of R/NCDs and B/NSCDs@Cu without ziram, respectively. As depicted in Fig. 3A, upon increasing the ziram concentration, the fluorescence intensity of B/NSCDs@Cu at 400 nm and R/NCDs at 610 nm decreased. Consequently, the fluorescence intensity ratio  $(\Delta F/\Delta F_0)$  gradually increased as the ziram concentration increased. A linear relationship was noted in the concentration range of 20.0 - 1000.0 mg mL<sup>-1</sup> (Fig. 3B), with the corresponding linear regression equation:  $\Delta F/\Delta F_0 = 0.0005$ [ziram] + 0.0003 ( $R^2 = 0.9935$ ). To determine the limit of detection (LOD) for ziram, the following formula was employed:  $3\sigma/k$ , where  $\sigma$ represents the standard deviation, and k denotes the slope of the regression equation obtained from the calibration curve. The LOD for ziram was found to be as low as  $6.22 \text{ ng mL}^{-1}$ , indicating the high sensitivity of the proposed method. A comparison between the proposed

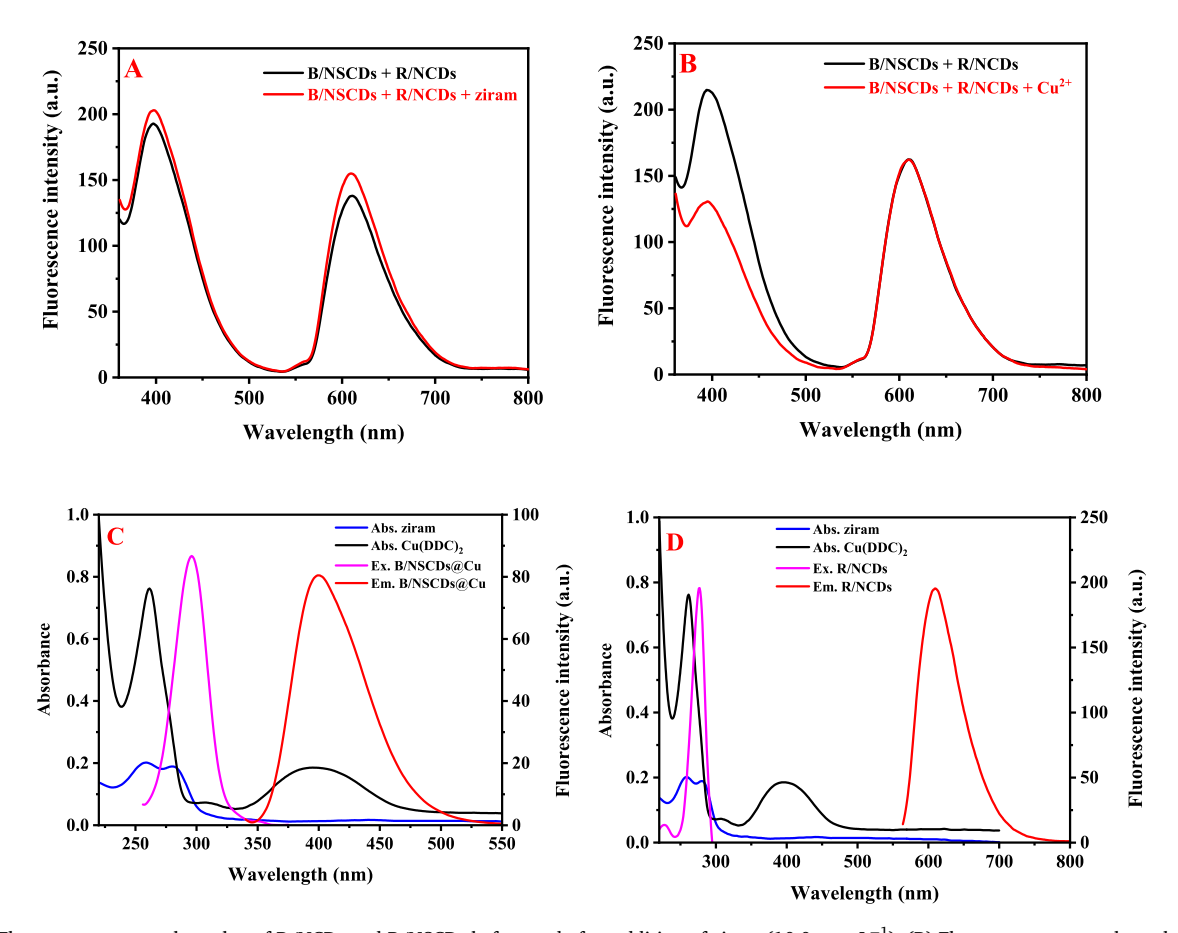


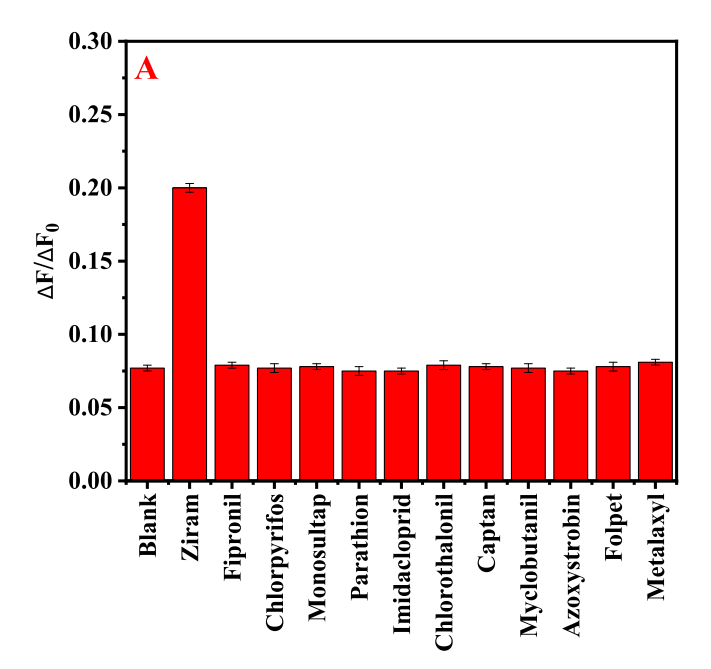
Fig. 4. (A) Fluorescence spectral overlay of R/NCDs and B/NSCDs before and after addition of ziram (10.0  $\mu$ g mL<sup>-1</sup>), (B) Fluorescence spectral overlay of R/NCDs and B/NSCDs before and after addition of Cu<sup>2+</sup> (10.0  $\mu$ g mL<sup>-1</sup>), (C) The overlay of the excitation and fluorescence spectra of B/NSCDs, along with the absorption spectra overlay of ziram and Cu(DDC)<sub>2</sub> and (D) The overlay of the excitation and fluorescence spectra of R/NCDs, along with the absorption spectra overlay of ziram and Cu(DDC)<sub>2</sub>.

method and previously reported fluorometric methods for ziram quantitation is presented in Table 1. The proposed dual quenching method offers high sensitivity and a wide linear range for ziram detection, comparable to or better than many reported techniques. It provides advantages like simplicity, cost-effectiveness, and avoidance of potential toxicity concerns. While fluorometric methods using other CDs generally offer good sensitivity, they may face challenges related to complex synthesis. Traditional techniques like Flame-AAS, Spectrophotometry, and SERS can suffer from interferences, higher detection limits, or complex sample preparation. The proposed method's dual quenching strategy presents a promising approach, combining high sensitivity and selectivity with potential for portable device development.

#### 3.6. Mechanism of detection of ziram

Upon the addition of ziram to the B/NSCDs@Cu and R/NCDs system, the fluorescence of R/NCDs and B/NSCDs@Cu is quenched. To acquire a comprehensive understanding of the fluorescence quenching mechanism, a series of experiments were conducted. Addition of ziram (10.0 µg mL<sup>-1</sup>) can quench the fluorescence of B/NSCDs slightly and have moderate quenching effect on R/NCDs which affect sensitivity of determination as shown on Fig. 4A. To overcome this sensitivity problem, Cu<sup>2+</sup> are added to the system to form the B/NSCDs@Cu. Addition of Cu<sup>2+</sup> to this system causes fluorescence quenching of B/NSCDs but has no effect on R/NCDs as shown in Fig. 4B. The possible reason that B/ NSCDs respond to addition of Cu<sup>2+</sup> is that B/NSCDs exhibit a negative surface charge due to presence of carboxylate, hydroxyl, and sulfonyl groups. These surface characteristics enhance the complexation ability with Cu<sup>2+</sup>. The quenching of B/NSCDs by copper ions does not pose any issues in our determination because the B/NSCDs@Cu system is regarded as a unified fluorescence system, regardless of the initial fluorescence intensity. Upon addition of ziram to this dual emission system, bright yellow color appears of copper dimethyldithiocarbamate (Cu (DDC)2). The yellow color produced led to an increased degree of spectral overlap of the produced complex with the excitation and emission spectra of B/NSCDs (Fig. 4C). Furthermore, the spectral overlap became even more significant with the excitation spectrum of R/ NCDs (Fig. 4D). The formation of yellow color may be attributed to the displacement of Zn<sup>2+</sup> from ziram by Cu<sup>2+</sup> and the strong binding ability of dimethyldithiocarbamate to  $Cu^{2+}$  more than  $Zn^{2+}$  [55,56]. The dithiocarbamate moiety in ziram has a high affinity for Cu<sup>2+</sup>, resulting in the formation of a stable copper-dimethyl dithiocarbamate complex. Consequently, the Cu<sup>2+</sup> initially bound to the B/NSCDs are displaced, leading to significant fluorescence quenching due to yellow color formation.

Fluorescence lifetime experiments were performed to better understand the quenching mechanisms responsible for the observed phenomena [57-60]. For the B/NSCDs@Cu system, the overlap in spectra between the absorption of Cu(DDC)2 and the excitation and emission spectra of B/NSCDs could potentially arise from either an inner filter effect (IFE) or Förster resonance energy transfer (FRET). To distinguish between these two mechanisms, the fluorescence decay time of B/ NSCDs@Cu was measured in the absence and presence of Cu(DDC)2. No change in the fluorescence lifetime was detected (Fig. S4A), supporting the occurrence of an IFE rather than FRET. In the case of R/NCDs, the spectral overlap occurred only between the absorption spectrum of Cu (DDC)<sub>2</sub> and the excitation spectrum of R/NCDs, suggesting the possibility of an IFE. To confirm this, fluorescence lifetime measurements were conducted for the R/NCDs system. Again, no change in the fluorescence lifetime was identified in the presence of Cu(DDC)2 (Fig. S4B), confirming the occurrence of an IFE. In addition to the inner filter effect, static quenching also plays a role in the fluorescence quenching process in the B/NSCDs@Cu and R/NCDs systems upon ziram addition. This was proven by employing the Stern-Volmer equation:  $F_0/F = 1 +$  $K_{SV}[ziram]$ , where [ziram] is the ziram concentration, and  $F_0$  and F are the fluorescence intensities without and with ziram, respectively. The



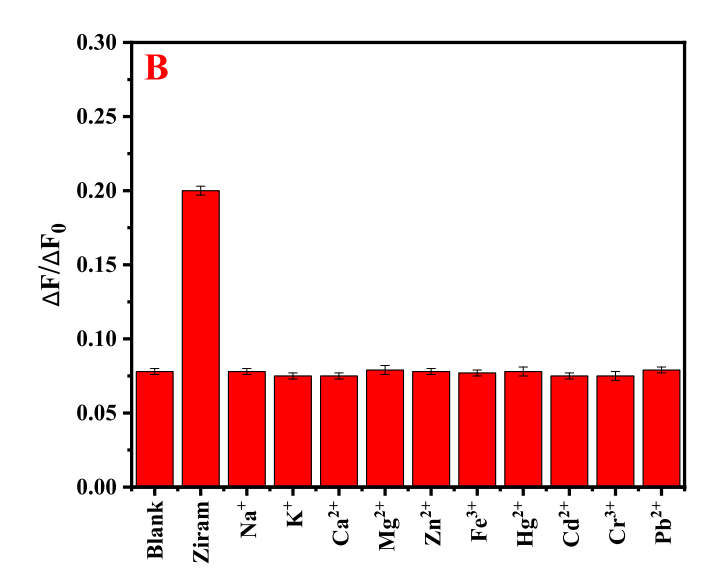


Fig. 5. The effect of different (A) fungicides and insecticides on the difference of fluorescence intensity ratio ( $\Delta F/\Delta F_0$ ) of B/NSCDs@Cu and R/NCDs system, and (B) metal ions on ( $\Delta F/\Delta F_0$ ) of B/NSCDs@Cu and R/NCDs system.

quenching constant ( $K_{SV}$ ) decreased with increasing temperature (Fig. S4C and D), suggesting that the static quenching, involving the formation of non-fluorescent ground-state complexes between the carbon dots and ziram, is favored at lower temperatures.

#### 3.7. Selectivity

The selectivity of the B/NSCDs@Cu and R/NCDs fluorescence system toward ziram detection was investigated by evaluating its response to various fungicides and insecticides commonly used in agriculture. The selection of these specific compounds was based on their widespread use and potential co-occurrence with ziram due to common application in agricultural environments. The fungicides and insecticides evaluated included fipronil, chlorpyrifos, monosultap, parathion, imidacloprid (insecticides), and chlorothalonil, captan, myclobutanil, azoxystrobin, folpet, and metalaxyl (fungicides). These compounds exhibit a diverse range of chemical properties and mechanisms of action, making them

**Table 2** Recovery of ziram from treated water, apple and wheat grains samples by the proposed method and reported method (n = 3).

Samples	Added	Proposed method	Proposed method		Reported method [50]	
	(ng mL <sup>-1</sup> )	Found (ng mL <sup>-1</sup> )	Recovery (%) ± RSD (%)	Found (ng mL <sup>-1</sup> )	Recovery (%) ± RSD (%)	
Tap water	0	Not detected		Not detected		
	20	19.52	$97.60 \pm 1.25$	20.12	$100.60\pm2.11$	
	100	98.35	$98.35 \pm 2.34$	99.65	$99.65\pm1.99$	
2	0	Not detected		Not detected		
	20	19.87	$99.35 \pm 1.98$	19.96	$99.80\pm2.05$	
	100	100.22	$100.22 \pm 2.98$	99.03	$99.03 \pm 2.66$	
Wheat grain	0	Not detected		Not detected		
	20	20.35	$101.75 \pm 2.78$	19.75	$98.75 \pm 2.38$	
	100	99.25	$99.25\pm2.33$	98.47	$98.47\pm2.98$	
Apple	0	Not detected		Not detected		
	20	20.45	$102.25 \pm 2.45$	20.02	$101.00\pm2.29$	
	100	98.56	$98.56 \pm 2.47$	99.61	$99.61 \pm 1.71$	

suitable for assessing the specificity of the ziram reported detection method in various matrices such as water, and foodstuffs. As shown in Fig. 5A, the change in fluorescence ratio ( $\Delta F/\Delta F_0$ ) induced by ziram was remarkably higher than that of the investigated fungicides and insecticides at concentrations up to 10.0 µg mL<sup>-1</sup>. The observed results align with the proposed detection mechanism, which can be elucidated by the specific interactions occurring between the Cu<sup>2+</sup> ions associated with the B/NSCDs@Cu system and the dithiocarbamate functional groups present in the ziram molecule. Additionally, the selectivity of the proposed method was evaluated by studying the effect of common metal cations present in real sample matrices such as apples, grains, and water. As depicted in Fig. 5B, these metal cations showed negligible influence on the fluorescence response, indicating that the proposed method exhibits excellent selectivity for ziram detection, even in the presence of potentially interfering metal ions found in the studied matrices. Therefore, the B/NSCDs@Cu and R/NCDs fluorescence system demonstrated excellent selectivity toward ziram, with minimal interference from other fungicides, insecticides, and common metal cations, making it a potential method for the specific detection and analysis of ziram in various agricultural matrices.

## 3.8. Applications

The proposed ratiometric fluorescence method based on B/ NSCDs@Cu and R/NCDs was applied to determine the presence of ziram in various matrices, including tap water, river water, wheat grains, and apple samples. To evaluate the method's performance, known amounts of ziram were spiked into these sample matrices. The samples were initially confirmed to be free of ziram and other studied fungicides. The recovery of ziram from the fortified samples was determined by comparing the measured concentrations to the known spiked amounts. The results of these determinations are presented in Table 2. The recoveries obtained for ziram in the different sample matrices were excellent, ranging from 97.60 % to 102.25 %. These values indicate the high accuracy and reliability of the proposed approach for the quantitative determination of ziram in various environmental and food samples. To establish the baseline concentrations, untreated samples were analyzed as references. The results confirmed the absence of ziram in the unspiked samples, further validating the accuracy of the method.

Matching results from other sensitive fluorometric methods suggest that the newly developed sensing platform ensures reliable accuracy and precision for the quantitative determination of ziram in diverse samples [50].

#### 4. Conclusions

In conclusion, this work presents a highly sensitive and selective method for the detection of the fungicide ziram by exploiting the dual fluorescence quenching of R/NCDs and B/NSCDs@Cu induced by the formation of copper dimethyldithiocarbamate Cu(DDC)2. The displacement of zinc ions from ziram by copper ions bound to the carbon dots results in the generation of the yellow-colored complex, which acts as an efficient quencher of the carbon dot emissions. The proposed method exhibited remarkable sensitivity across a wide concentration range, enabling trace-level detection of ziram. Additionally, the excellent selectivity and high recovery rates achieved when the method was applied to real samples, such as apples, grains, and water matrices, highlight its potential for practical applications in environmental monitoring and food safety assessments. The combination of high sensitivity, selectivity, and applicability to diverse sample matrices makes this carbon dot-based dual quenching approach a promising tool for the rapid and accurate detection of ziram. Moreover, the simplicity and cost-effectiveness of the method, along with the unique optical properties and biocompatibility of carbon dots, open up opportunities for further development and adaptation to other analyte detection scenarios. The key advantages of the carbon dot-based dual quenching approach include wide concentration range, trace-level detection, and excellent performance in real samples. However, the synthesis complexity and multiple components involved pose challenges. Future research could simplify carbon dot synthesis, develop multiplexed sensing platforms, and integrate portable devices for on-site monitoring.

#### CRediT authorship contribution statement

Khalid Alhazzani: Visualization, Validation, Investigation, Funding acquisition, Data curation. Ahmed Z. Alanazi: Writing – review & editing, Visualization, Software, Funding acquisition, Formal analysis, Conceptualization. Aya M. Mostafa: . James Barker: Visualization, Software, Project administration, Funding acquisition, Conceptualization. Hossieny Ibrahim: Writing – original draft, Validation, Resources, Investigation, Conceptualization. Mohamed M. El-Wekil: . Al-Montaser Bellah H. Ali: Data curation, Formal analysis, Methodology, Project administration, Software, Supervision, Validation, Writing – original draft, Writing – review & editing.

#### Declaration of competing interest

The authors declare that they have no known competing financial interests or personal relationships that could have appeared to influence

the work reported in this paper.

#### Data availability

Data will be made available on request.

#### Acknowledgments

The authors would like to extend their appreciation to the Researchers Supporting Project number (RSPD2024R593) at King Saud University, Riyadh, Saudi Arabia.

#### Appendix A. Supplementary data

Supplementary data to this article can be found online at https://doi.org/10.1016/j.microc.2024.111092.

#### References

- D.M. Janz, Dithiocarbamates, in: P. Wexler (Ed.), Encyclopedia of Toxicology (third Edition), Academic Press, Oxford, 2014, pp. 212–214.
- [2] M.M. Andrianova, I.V. Alekseev, Carcinogenic properties of the pesticides Sevin, Maneb, Ziram and Zineb, Vopr Pitan 29 (1970) 71–74.
- [3] M.H. Prasad, P.P. Reddy, Rubber Industry, Toxicity of Work Environment, in: M. Corn (Ed.), Handbook of Hazardous Materials, Academic Press, Boston, 1993, pp. 639–648.
- [4] J. Harrigan, D.F. Brambila, P. Meera, D.E. Krantz, F.E. Schweizer, The environmental toxicant ziram enhances neurotransmitter release and increases neuronal excitability via the EAG family of potassium channels, Neurobiol. Dis. 143 (2020) 104977.
- [5] J. Liu, Y. Wang, Y. Fang, C. Ni, L. Ma, W. Zheng, S. Bao, X. Li, Q. Lian, R.-S. Ge, Gestational exposure to ziram disrupts rat fetal Leydig cell development, Chemosphere 203 (2018) 393–401.
- [6] J.M. Mack, T.M. Moura, D. Lanznaster, F. Bobinski, C.M. Massari, T.B. Sampaio, A. E. Schmitz, L.F. Souza, R. Walz, C.I. Tasca, A. Poli, R.L. Doty, A.L. Dafre, R. D. Prediger, Intranasal administration of sodium dimethyldithiocarbamate induces motor deficits and dopaminergic dysfunction in mice, Neurotoxicology 66 (2018) 107-120
- [7] F. Cao, C.L. Souders, P. Li, O. Adamovsky, S. Pang, L. Qiu, C.J. Martyniuk, Developmental toxicity of the fungicide ziram in zebrafish (Danio rerio), Chemosphere 214 (2019) 303–313.
- [8] S. Agarwal, S.G. Aggarwal, P. Singh, Quantification of ziram and zineb residues in fog-water samples, Talanta 65 (2005) 104–110.
- [9] J.T. Phinney, K.W. Bruland, Trace metal exchange in solution by the fungicides Ziram and Maneb (dithiocarbamates) and subsequent uptake of lipophilic organic zinc, copper and lead complexes into phytoplankton cells, Environ. Toxicol. Chem. 16 (1997) 2046–2053.
- [10] K.W. Weissmahr, D.L. Sedlak, Effect of metal complexation on the degradation of dithiocarbamate fungicides, Environ. Toxicol. Chem. 19 (2000) 820–826.
- [11] T.O. Ajiboye, T.T. Ajiboye, R. Marzouki, D.C. Onwudiwe, The versatility in the applications of dithiocarbamates, Int. J. Mol. Sci. 23 (2022) 1317.
- [12] Z. Vryzas, E.N. Papadakis, E. Papadopoulou-Mourkidou, Microwave-assisted extraction (MAE)—acid hydrolysis of dithiocarbamates for trace analysis in tobacco and peaches, J. Agric. Food Chem. 50 (2002) 2220–2226.
- [13] E.D. Caldas, M.H. Conceição, M.C.C. Miranda, L.C.K.R. de Souza, J.F. Lima, Determination of dithiocarbamate fungicide residues in food by a spectrophotometric method using a vertical disulfide reaction system, J. Agric. Food Chem. 49 (2001) 4521–4525.
- [14] A.R. Cassella, S. Garrigues, R.C. de Campos, M. de la Guardia, Fourier transform infrared spectrometric determination of Ziram, Talanta 54 (2001) 1087–1094.
- [15] E. Yilmaz, M. Soylak, Preparation and characterization of magnetic carboxylated nanodiamonds for vortex-assisted magnetic solid-phase extraction of ziram in food and water samples, Talanta 158 (2016) 152–158.
- [16] N.H. Petha, R.S. Lokhande, D.T. Seshadri, R.M. Patil, T.S. Bhagat, J.G. Patil, A simple pre-column derivatization method for the determination of mancozeb technical (fungicide) by reverse phase HPLC-UV, Anal. Methods 9 (2017) 4702–4708.
- [17] O.J. de Blas, J.L.P. de Paz, J.H. Méndez, Indirect determination of diethyldithiocarbamate by atomic absorption spectrometry with continuous extraction: application to the determination of the fungicide ziram, J. Anal. At. Spectrom. 5 (1990) 693–696.
- [18] L. Mathew, M.L.P. Reddy, T.P. Rao, C.S.P. Iyer, A.D. Damodaran, Differential pulse anodic stripping voltammetric determination of ziram (a dithiocarbamate fungicide), Talanta 43 (1996) 73–76.
- [19] J. Chen, F. Fu, S. Wu, J. Wang, Z. Wang, Simultaneous detection of zinc dimethyldithiocarbamate and zinc ethylenebisdithiocarbamate in cabbage leaves by capillary electrophoresis with inductively coupled plasma mass spectrometry, J. Sep. Sci. 40 (2017) 3898–3904.
- [20] I. Cesarino, F.C. Moraes, M.R.V. Lanza, S.A.S. Machado, Electrochemical detection of carbamate pesticides in fruit and vegetables with a biosensor based on

- acetylcholinesterase immobilised on a composite of polyaniline–carbon nanotubes, Food Chem. 135 (2012) 873–879.
- [21] D. Liu, W. Chen, J. Wei, X. Li, Z. Wang, X. Jiang, A highly sensitive, dual-readout assay based on gold nanoparticles for organophosphorus and carbamate pesticides, Anal. Chem. 84 (2012) 4185–4191.
- [22] S.A. Ghoto, M.Y. Khuhawar, T.M. Jahangir, J.u.D. Mangi, Applications of copper nanoparticles for colorimetric detection of dithiocarbamate pesticides, J. Nanostructure Chem. 9 (2019) 77–93.
- [23] Q. Fu, C. Long, L. Qin, Z. Jiang, T. Qing, P. Zhang, B. Feng, Fluorescent and colorimetric dual-mode detection of tetracycline in wastewater based on heteroatoms-doped reduced state carbon dots, Environ. Pollut. 283 (2021) 117109.
- [24] C. Long, Z. Jiang, J. Shangguan, T. Qing, P. Zhang, B. Feng, Applications of carbon dots in environmental pollution control: A review, J. Chem. Eng. 406 (2021) 126848.
- [25] Y. Chen, X. Sun, X. Wang, W. Pan, G. Yu, J. Wang, Carbon dots with red emission for bioimaging of fungal cells and detecting Hg<sup>2+</sup> and ziram in aqueous solution, Spectrochim. Acta A Mol. Biomol. Spectrosc. 233 (2020) 118230.
- [26] K. Alhazzani, A.Z. Alanazi, A.M. Mostafa, J. Barker, M.M. El-Wekil, H.A.A. M. Bellah, A selective dual quenching sensor (EY/BG@CDs) for simultaneous monitoring of gentamicin and ketorolac levels in plasma: a highly efficient platform that caters to the needs of therapeutic drug monitoring, RSC Adv. 13 (2023) 28940–28950.
- [27] S.A. Alkahtani, A.M. Mahmoud, Y.S. Alqahtani, A.-M.-B.-H. Ali, M.M. El-Wekil, Selective detection of rutin at novel pyridinic-nitrogen-rich carbon dots derived from chicken feet biowaste: The role of bovine serum albumin during the assay, Spectrochim. Acta A Mol. Biomol. Spectrosc. 303 (2023) 123252.
- [28] A.M. Mahmoud, S.A. Alkahtani, Y.S. Alqahtani, R.M.K. Mohamed, M.M. El-Wekil, A.-M.-B.-H. Ali, Ultrasensitive and selective determination of naringin using eggplant peel- derived nitrogen doped-carbon dots after extraction with Amberlite IRA-400: Evaluation the bitterness of grapefruit juice, Microchem. J. 194 (2023) 109358.
- [29] A.Z. Alanazi, K. Alhazzani, A.M. Mahmoud, A.-M.-B.-H. Ali, M.M. El-Wekil, Advanced fluorescence-based determination of carboplatin, a potent anticancer agent, with tripeptide-functionalized copper nanoclusters, Microchem. J. 199 (2024) 110000.
- [30] A.Z. Alanazi, K. Alhazzani, A.M. Mostafa, J. Barker, M.M. El-Wekil, A.-M.-B.-H. Ali, Selective and reliable fluorometric quantitation of anti-cancer drug in real plasma samples using nitrogen-doped carbon dots after MMIPs solid phase microextraction: Monitoring methotrexate plasma level, J. Pharm. Biomed. Anal. 238 (2024) 115862.
- [31] K. Alhazzani, A.Z. Alanazi, A.M. Mostafa, J. Barker, M.M. El-Wekil, A.-M.-B.-H. Ali, A dual emissive silver-riboflavin complex and nitrogen-doped carbon dot nanoprobe for ratiometric detection of glutathione, Microchem. J. 199 (2024) 109996.
- [32] Y.S. Alqahtani, A.M. Mahmoud, M.M. El-Wekil, A.-M.-B.-H. Ali, Selective fluoride detection based on modulation of red emissive carbon dots fluorescence by zirconium-alizarin complex: Application to Nile River water and human saliva samples, Microchem. J. 198 (2024) 110184.
- [33] A.Z. Alanazi, K. Alhazzani, A.M. Mostafa, J. Barker, M.M. El-Wekil, A.-M.-B.-H. Ali, Highly selective fluorometric detection of streptokinase via fibrinolytic release of photoluminescent carbon dots integrated into fibrin clot network, Microchem. J. 197 (2024) 109800.
- [34] J.V. Rohit, V.N. Mehta, A.B. Patel, H. Tabasum, G. Spolia, Chapter 9 Carbon dots-based fluorescence spectrometry for pesticides sensing, in: S.K. Kailasa, C. M. Hussain (Eds.), Carbon Dots in Analytical Chemistry, Elsevier, 2023, pp. 97–108.
- [35] P. Mandal, D. Sahoo, P. Sarkar, K. Chakraborty, S. Das, Fluorescence turn-on and turn-off sensing of pesticides by carbon dot-based sensor, New J. Chem. 43 (2019) 12137–12151.
- [36] Z. Wang, Y. Li, B. Zhang, X. Gao, M. Shi, S. Zhang, S. Zhong, Y. Zheng, X. Liu, Functionalized carbon dot-delivered RNA nano fungicides as superior tools to control phytophthora pathogens through plant RdRP1 mediated spray-induced gene silencing, Adv. Funct. Mater. 33 (2023) 2213143.
- [37] H.W. Chu, B. Unnikrishnan, A. Anand, Y.W. Lin, C.C. Huang, Carbon quantum dots for the detection of antibiotics and pesticides, J. Food Drug Anal. 28 (2020) 539–557.
- [38] J. Ahlawat, G. Henriquez, A. Varela-Ramirez, R. Fairman, M. Narayan, Gelatin-derived carbon quantum dots mitigate herbicide-induced neurotoxic effects in vitro and in vivo, Biomater. Adv. 137 (2022) 212837.
- [39] K. Alhazzani, A.Z. Alanazi, A.M. Mostafa, J. Barker, M.M. El-Wekil, A.B.H. Ali, Cobalt-modulated dual emission carbon dots for ratiometric fluorescent vancomycin detection, RSC Adv. 14 (2024) 5609–5616.
- [40] K. Alhazzani, A.Z. Alanazi, A.M. Mostafa, J. Barker, M.M. El-Wekil, A.B.H. Ali, Selective fluorescence turn-on detection of combination cisplatin-etoposide chemotherapy based on N-CDs/GSH-CuNCs nanoprobe, RSC Adv. 14 (2024) 2380–2390.
- [41] B.L. Turner, K.M. Kilgour, S.J. Stine, M. Daniele, S. Menegatti, Dual-affinity ratiometric quenching (DARQ) Assay for the quantification of therapeutic antibodies in CHO-S cell culture fluids, Anal. Chem. 92 (2020) 16274–16283.
- [42] Q. Zhang, Z. Cui, Q. Wang, G. Zheng, Construction of a ratiometric probe with dual quenching mechanisms for selectively imaging intracellular sulfur dioxide overcoming the interference from cysteine, Sens. Actuators B: Chem. 295 (2019) 70, 95
- [43] L. Luo, X. Liu, X. Bi, L. Li, T. You, Dual-quenching effects of methylene blue on the luminophore and co-reactant: Application for electrochemiluminescent-

- electrochemical ratiometric zearalenone detection, Biosens. Bioelectron. 222 (2023) 114991.
- [44] A.M. Mahmoud, Y.S. Alqahtani, M.M. El-Wekil, A.-M.-B.-H. Ali, Ratiometric sensing of azithromycin and sulfide using dual emissive carbon dots: A turn on-offon approach, J. Fluoresc. (2024).
- [45] H. Luo, Y. Huang, K. Lai, B.A. Rasco, Y. Fan, Surface-enhanced Raman spectroscopy coupled with gold nanoparticles for rapid detection of phosmet and thiabendazole residues in apples, Food Control 68 (2016) 229–235.
- [46] A. Kumar Malik, W. Faubel, Capillary electrophoretic determination of zinc dimethyldithiocarbamate (Ziram) and zinc ethylenebisdithiocarbamate (Zineb), Talanta 52 (2000) 341–346.
- [47] A.H. Rageh, F.A.M. Abdel-aal, S.A. Farrag, A.-M.-B.-H. Ali, A surfactant-based quasi-hydrophobic deep eutectic solvent for dispersive liquid-liquid microextraction of gliflozins from environmental water samples using UHPLC/ fluorescence detection, Talanta 266 (2024) 124950.
- [48] B. Zhao, H. Ma, M. Zheng, K. Xu, C. Zou, S. Qu, S. Tan, Narrow-bandwidth emissive carbon dots: A rising star in the fluorescent material family, Carbon Energy 4 (2022) 88–114.
- [49] B.D. Mansuriya, Z. Altintas, Carbon dots: Classification, properties, synthesis, characterization, and applications in health care-an updated review (2018–2021), Nanomaterials (Basel) 11 (2021) 2525.
- [50] L. Yang, X. Zhang, J. Wang, H. Sun, L. Jiang, Double-decrease of the fluorescence of CdSe/ZnS quantum dots for the detection of zinc(II) dimethyldithiocarbamate (ziram) based on its interaction with gold nanoparticles, Mikrochim. Acta 185 (2018) 472.
- [51] S. Chen, M. Huang, M. Huang, L. Feng, Fluorometric determination of ziram using CsPbBr<sub>3</sub> quantum dots, Mikrochim. Acta 188 (2021) 390.

- [52] Q. Wei, L. Zhang, C. Song, H. Yuan, X. Li, Quantitative detection of dithiocarbamate pesticides by surface-enhanced Raman spectroscopy combined with an exhaustive peak-seeking method, Anal. Methods 13 (2021) 1479–1488.
- [53] N. Hussain, H. Pu, A. Hussain, D.-W. Sun, Rapid detection of ziram residues in apple and pear fruits by SERS based on octanethiol functionalized bimetallic coreshell nanoparticles, Spectrochim. Acta A Mol. Biomol. Spectrosc. 236 (2020) 118357.
- [54] L. Mathew, T.P. Rao, C.S.P. Iyer, A.D. Damodaran, Spectrophotometric determination of ziram (dithiocarbamate fungicide) by thiocyanate and rhodamine 6G method, Talanta 42 (1995) 41–43.
- [55] B. Cvek, V. Milacic, J. Taraba, Q.P. Dou, Ni(II), Cu(II), and Zn(II) diethyldithiocarbamate complexes show various activities against the proteasome in breast cancer cells, J. Med. Chem. 51 (2008) 6256–6258.
- [56] W. Liu, H. Duan, D. Wei, B. Cui, X. Wang, Stability of diethyl dithiocarbamate chelates with Cu(II), Zn(II) and Mn(II), J. Mol. Struct. 1184 (2019) 375–381.
- [57] Y. Liu, X. Su, L. Chen, H. Liu, C. Zhang, J. Liu, J. Hao, Y. Shangguan, G. Zhu, Green preparation of carbon dots from Momordica charantia L. for rapid and effective sensing of p-aminoazobenzene in environmental samples, Environ. Res. 198 (2021) 111279.
- [58] Y. Liu, P. Zhou, Y. Wu, X. Su, H. Liu, G. Zhu, Q. Zhou, Fast and efficient "on-off-on" fluorescent sensor from N-doped carbon dots for detection of mercury and iodine ions in environmental water, Sci. Total Environ. 827 (2022) 154357.
- [59] T. Rasheed, Carbon dots as robust class of sustainable and environment friendlier nano/optical sensors for pesticide recognition from wastewater, TrAC, Trends Anal. Chem. 160 (2023) 116957.
- [60] Y. Liu, X. Su, H. Liu, G. Zhu, G. Ge, Y. Wang, P. Zhou, Q. Zhou, Construction of ecofriendly dual carbon dots ratiometric fluorescence probe for highly selective and efficient sensing mercury ion, J. Environ. Sci. 148 (2025) 1–12.